Morphogenesis of polycrystalline dendritic patterns from evaporation of a reactive nanofluid sessile drop

Hua Wu, Wuge H. Briscoe**

School of Chemistry, University of Bristol, Cantock's Close, Bristol BS8 1TS, United Kingdom
E-mail: chzhw@bristol.ac.uk; wuge.briscoe@bristol.ac.uk

Keywords: coffee ring effect, evaporation controlled self-assembly, dendritic surface patterns, ZnO nanoparticles, Bénard-Marangoni flows

Abstract We report polycrystalline residual patterns with dendritic micromorphologies upon fast evaporation of a mixed-solvent sessile drop containing reactive ZnO nanoparticles. The molecular and particulate species generated *in situ* upon evaporative drying collude with and modify the Marangoni solvent flows and Bénard-Marangoni instabilities, as they undergo self-assembly and self-organisation under conditions far from equilibrium, leading to the ultimate hierarchical central cellular patterns surrounded by a peripheral coffee ring upon drying.

Facile formation of functional hierarchical surface patterns with tailored morphology is a central challenge in functional nano- and meso-scale materials research. A widely studied system for spontaneous pattern formation is evaporative drying of a sessile drop containing non-volatile particles.[1] The most familiar pattern is the "coffee ring", due to an outward capillary flow that shuttles dispersed particles towards the peripheral contact line where they get trapped.[2] Marangoni effects[3] may counteract this capillary flow,[4] and the residual pattern may be further influenced by instabilities triggered by a temperature gradient across the solvent layer that manifest in different convective patterns, e.g. the Bénard-Marangoni (BM) convection.[1e, 5] By controlling parameters such as evaporation rate, substrate chemistry, particle shape, size and concentration, droplet confinement, and surfactant addition, a plethora of patterns can be obtained, such as concentric rings,[6] polycrystalline dendrites,[7] uniform

deposits,[8] and polygonal particle networks.[5c] The coffee ring effect has also been exploited in applications, e.g. inkject printing[9] and fabrication of sensors[10] and transparent conductors.[10b] Another related research area involves precipitation and crystallisation from a drying sessile drop of aqueous salt solution[11], where capillary flows and supersaturation of salts upon evaporation led to residual patterns of recrystalised salts.

In those previous studies involving particulate dispersions, the dispersed non-volatile particles were inert; mechanistically, the pattern formation resulted from a competition between inter-particle forces[12] and capillary and convective solvent flows. It remains little understood how reactive particles may alter evaporation induced patterns, for *in situ* generated molecular and particulate species can affect the solvent flows and thus the residual pattern. Here we show that, upon fast evaporation (several minutes) of a ZnO nanoparticle dispersion in chloroform/methanol/isobutylamine mixture (denoted as CM/iB), hierarchical polycrystalline patterns with dendritic micromorphologies were formed, comprising a central region of cellular patterns surrounded by a peripheral coffee ring. We elucidate a formation mechanism for such hierarchical surface patterns as follows. ZnO nanoparticles undergo rapid chemical transformation into isobutylamine-ZnOH molecular complexes (iZMCs) of sub-nanometer in size, which further self-assemble into nanoclusters. These surface active iZMCs and clusters accumulate at the drop surface and the peripheral contact line. As the drop thins, BM flows are triggered, and iZMC-cluster coalescence along multiple BM flows leads to the formation of the central cellular patterns. Concurrently, this dendritic cluster growth also occurs at the receding peripheral contact line. Further drying drives iZMC organisation into crystal lattices in the micro-dendrites in the final hierarchical polycrystalline surface structures. We also show that the micro-morphological details of the dendrites in the residual pattern depended on the solvent composition, evaporation rate and ZnO nanoparticle concentration, thus confirming the interplay between the *in situ* generated iZMC clusters and the dynamic solvent flows under fast evaporation.

Figure 1 shows an example residual surface pattern after drying of a 400 μL droplet containing 1 mg/mL ZnO nanoparticles ~ 5-10 nm in size (**Supporting Information Figure S1**) in a solvent mixture of V_{CM}:V_{iB} = 5:1 on a 24 × 24 mm glass substrate, and evaporation took ~20 min to complete at 20^{o}C and a relative humidity (RH) of 65%. It comprised central cellular patterns surrounded by a coffee ring along the edge of the square substrate (**Figure 1a**). The microstructure of the coffee ring consisted of dendrites pointing inwards from the edge (**Figure 1b, c**), with the dendrite length corresponding approximately to the width of the coffee ring (~2 mm) and their ends interpenetrating. The central region showed 3D cellular patterns with dendrites radiating from the cell centre. The cells were approximately circular, interpenetrating at their boundaries and varying in size (200-500 μm; Figure 1d). SEM image in Figure 1e shows an individual cell (a magnified view of the white frame in **Figure 1d**) which resembled branched fronds of *Corallina elongata* (a red algae), with dendrites radiating from the centre and branches fanning radially outwards.

High resolution transmission electron microscopy (HRTEM) images of the constituent nanostructures collected at different evaporation time suggest that ZnO nanoparticles rapidly transformed into stable sub-nanoparticles (white dotted circles in **Figure 2a-c, e**) with a core size ~0.24 nm at the initial stage of solvent evaporation. XPS, ^{1}H NMR, and ^{13}C NMR analyses (Supporting Information SI.4 and **Figure S2-4**) confirm that these sub-nanoparticles

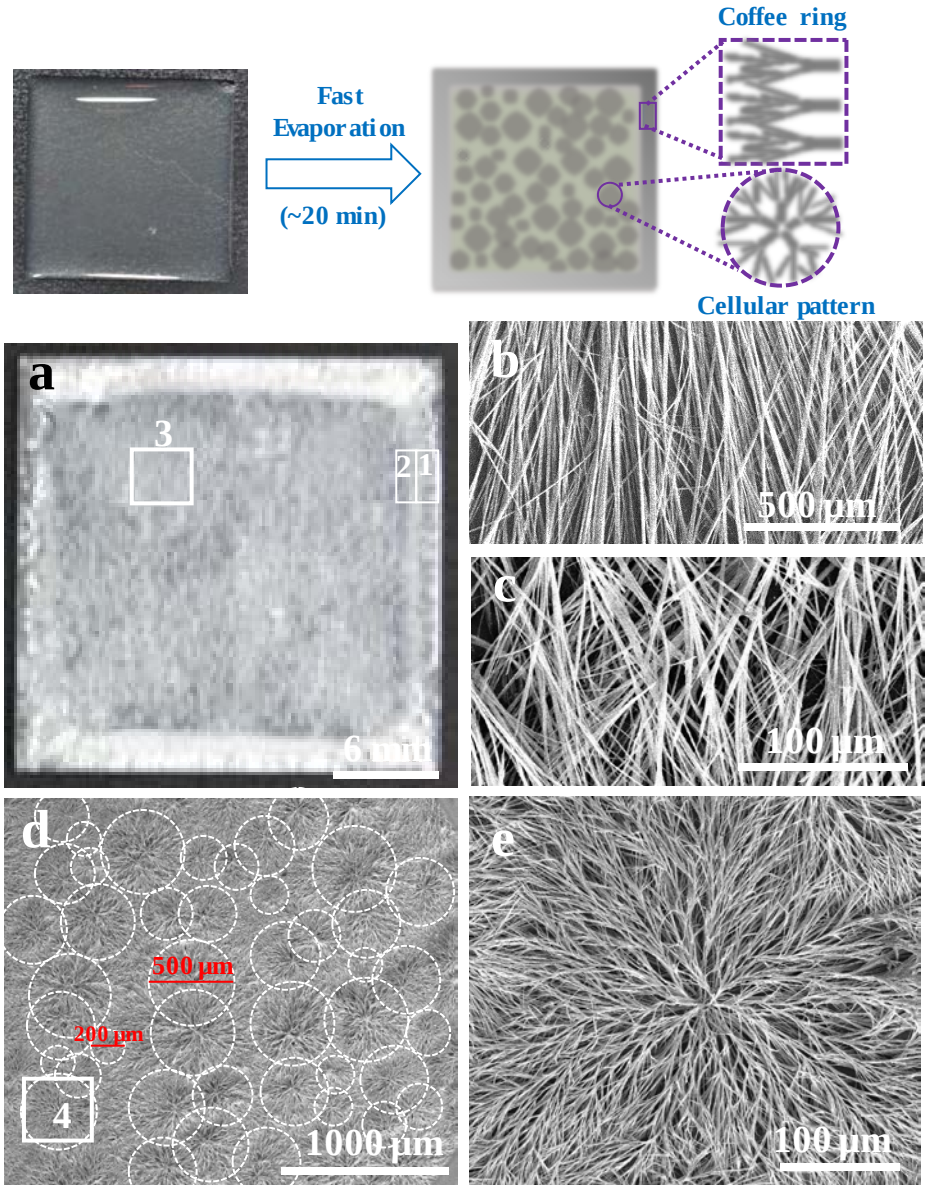

Figure 1. Residual surface pattern and SEM images from evaporative drying of a ZnO nanofluid droplet on a glass coverslip (24 × 24 mm). (**a**) Photographic image of a residual surface pattern; (**b and c**) Enlarged view of Regions 1 and 2 in (**a**); (**d**) Enlarged view of Region **3** in (a); (**e**) Enlarged view of Region **4** in (**d**); The nanofluid droplet was ~400 µL in volume, containing 1 mg/mL ZnO nanoparticles (Supporting Figure S1) in a mixture of chloroform and methanol (denoted CM; in a volume ratio of V_C:V_M = 10:3) and also isobutylamine in an overall volume ratio V_{CM}:V_{iB} = 5:1. Typically this evaporative drying process completed in ~20 min at 20°C and a relative humidity (RH) ~65%.

constituted solvated isobutylamine−ZnOH complexes (iZMCs).[13] At the evaporation time of ~12 min when no visible solvent remained (**Figure S5f**), the deposits were composed of aggregates with iZMCs in 2D square lattice packing (Figure 2c). At complete drying (~20 min), the filaments constituting the dendritic branches in the residual pattern were composed

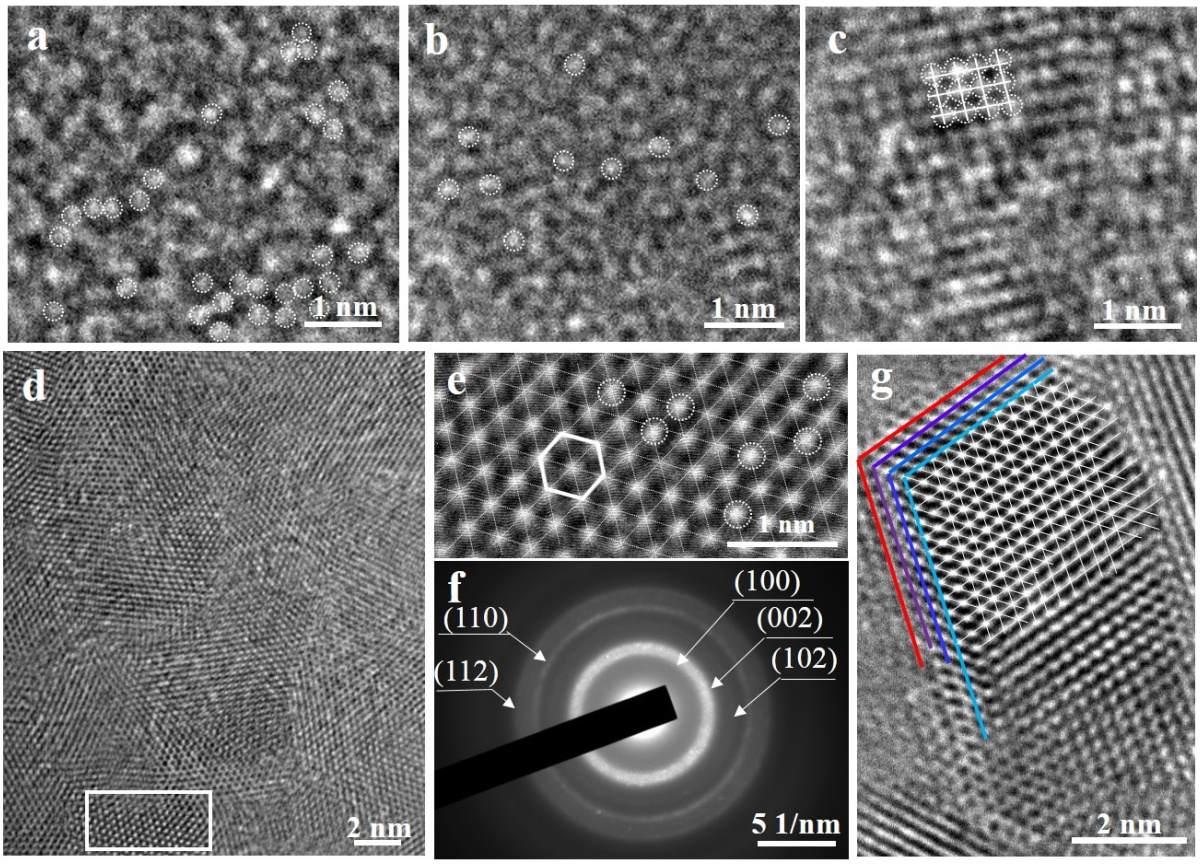

Figure 2. HRTEM images of the constituent nanostructures of a ZnO nanofluid droplet on a glass cover slip at different time intervals (Experimental protocol for HRTEM sample preparation of Figure 2a-c in Supporting information SI.3 and Figure 2d in Supporting information SI.4). (**a**) 2 min; (**b**) 4 min; (**c**) 12 min; (**d**) 20 min (complete drying); (**e**) The two-dimensional hexagonal lattices (as indicated by the red hexagon) in the white frame in (**d**); (**f**) SAED pattern of the 2D lattices in (**d**) assigned to different lattice planes; (**g**) HRTEM image of a single crystallite from completely dried deposits dispersed into ethanol, showing four lattice layers (as indicated with four coloured lines) all with iZMCs in a 2D hexagonal lattice structure. The dotted white circles in (a-c, e) indicate iZMCs.

of thin sheets/belts (**Figure S6g-h**). The HRTEM image in **Figure 2d** shows layered crystallites of varying domain sizes and orientations in a thin belt, characteristic for a polycrystalline structure, with the crystallites exhibiting a 2D hexagonal lattice (**Figure 2e**), representing the crystal structure in the final dried branches shown in **Figure 1b, c, e**. Selected area electron diffraction (SAED) indicates that this crystallographic structure was similar to that of hexagonal wurtzite (**Figure 2f**), with the diffuse SAED rings assigned to the (100), (002), (102), (110) and (112) planes, respectively. The HRTEM image in **Figure 2g** further reveals the layered 2D

hexagonal lattices in a single brick-like crystallite (coloured lines indicating different lattice layers).

To further elucidate the pattern formation mechanism, Cryo-TEM[14] at various evaporation time and video microscopy were used to monitor the temporal evolution of intermediate species within an evaporating droplet (**Figure 3a,b,d,e,g,h,j,k; Figure S6**), to complement the observations of the macroscopic pattern with the dendritic microscopic structure (**Figure 1**) and nanoscopic polycrystallinity (**Figure 2**). The proposed mechanism below as shown schematically in **Figure 3c,f,i,l** and **Figure 4a,b** is further supported by video microscopy (**Figure 4c-h, j-m; Supplementary Videos 1-3**), attempting to account for *in situ* generation of iZMCs and their clusters, cluster-induced capillary ripples at the drop surface, subsequent cluster coalescence tracking BM flows, and aggregation-based crystallization. We will specifically comment on assumptions made in suggesting the schematics in the discussion below.

At the initial stage of evaporation, ZnO nanoparticles were carried to the edge of the droplet by the outward capillary flow to the pinned contact line, where they underwent moisture-assisted transformation[15] into amphiphilic iZMCs with a core size ~0.24 nm (Figure 2a), which then formed solvated aggregates (of order 100 nm in size). Concurrently, the Marangoni flow spread the iZMC aggregates along the drop surface. This process of ZnO dissolution and chemical transformation into iZMCs was rapid. Cryo-TEM images at 2 min evaporation (**Figure 3a, b**) show the coexistence of solvated iZMC aggregates and undissolved ZnO nanoparticles (arrows in Figure 3b; also **Figure S6 a,b**), and the absence of any ZnO nanoparticles at just 4 min evaporation time (**Figure 3d**). Instead, iZMC aggregates were prominent (**Figure 3e**, dotted random shapes), with some iZMCs assembling into primary clusters of size 2-5 nm within the aggregates (the arrows in Figure 3e, and schematically shown in **Figure 3i**). We suggest that it is conceivable that these primary clusters were micelle- or vesicle-like, enclosing a polar core of methanol, isobutylamine and trace amounts of water and

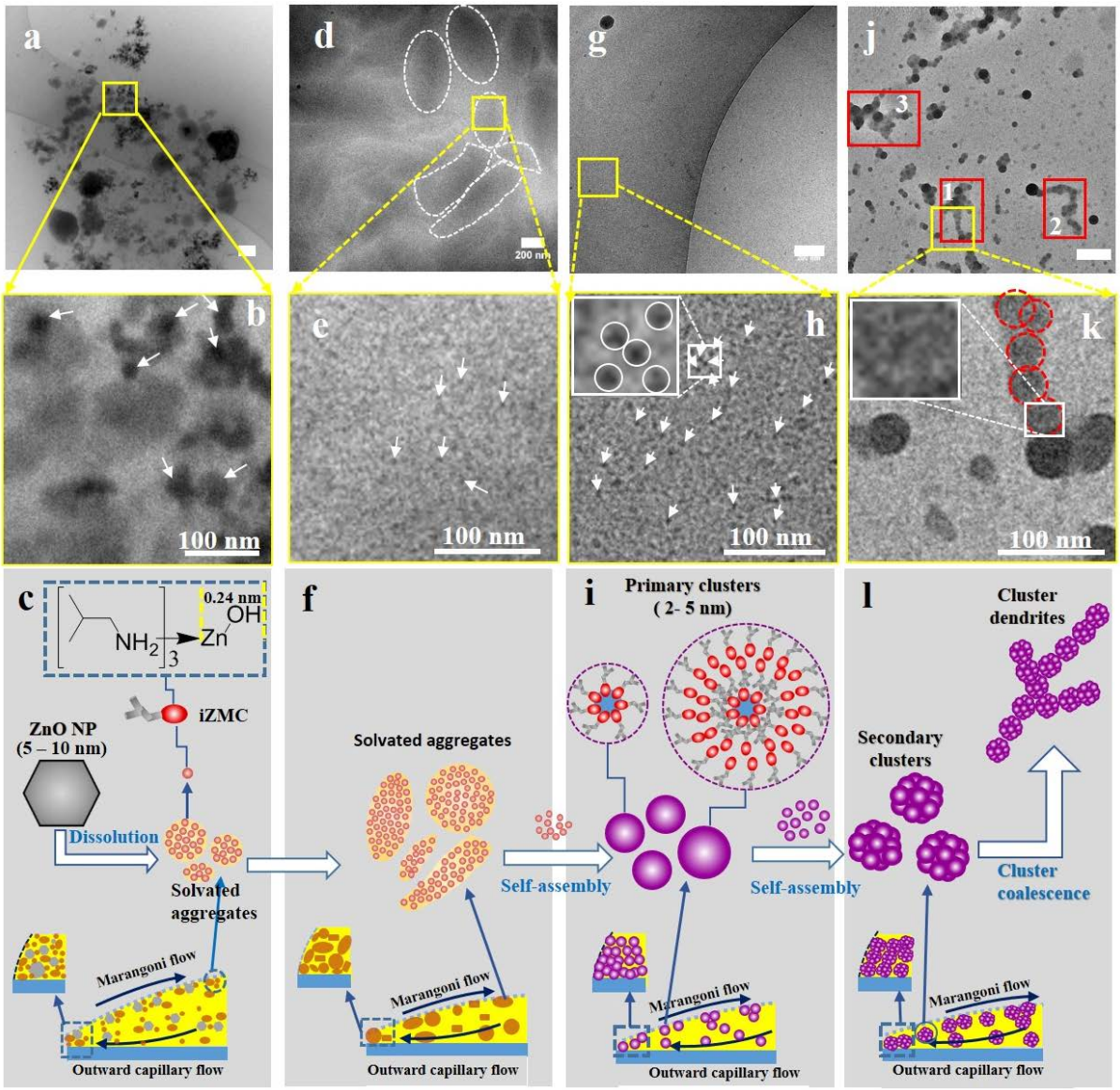

Figure 3. Cryo-TEM images of nano-constituents in an evaporating droplet at different time intervals: 2 min (a, b), 4 min (d, e), 6 min (g, h), and 8 min (j, k); and corresponding schematic of flows and cluster formation (c, f, i, and l). Images (b, e, h, k) are enlarged views of the white frames in a, d, g and j respectively. The insets in h and k show enlarged views of the white frames in h and k, respectively. The scale bars in a, d, g and j are 200 nm. The red frames (numbered 1-3) in Figure 3k highlight branched or linear aggregates of coalesced secondary clusters (red dashed circles in Figure 3l).

thus separating it from the surrounding nonpolar solvent. (Due to fast evaporation rate, it proved challenging to fully characterise the structure of such proposed primary cluster structure using classic X-ray and neutron scattering methods, which remains a focus of our continuing experimental effort.) At 6 min (**Figure 3g, h**), the iZMC aggregates were largely replaced by the primary clusters (arrows in Figure 3h and circles in the inset). At ~ 8 min (**Figure 3j, k**),

larger secondary clusters of diameter 30 nm (red dashed circles in Figure 3k) constituting a network of primary clusters (inset in Figure 3k) were observed, and their coalescence led to formation of branched or linear aggregates (red frames in Figure 3j). The cluster self-assembly process is likely pronounced at the droplet surface, due to their surface activity and also driven by evaporation.

As the drop thinned upon evaporation, BM instabilities were triggered,[8c, 16] consistent with the dendrite growth in the drop and also the observation of capillary ripples at the drop surface (**Videos 1 and 2**). [17] It is conceivable that the surface active iZMC clusters at the drop surface gave rise to a "skin" or crust, and vertical BM flows would bring upon cluster concentration inhomogeneity in this surface layer, the resulting stress instigating the capillary ripples.[18] Conversely, the enhanced surface elasticity due to the cluster crust made the capillary ripples readily observable in video microscopy (**Supporting Video 2**). A series of images (**Figure 4c-h**) extracted from Video 2 show that the cellular pattern formation, a manifestation of the solidification of ten BM convection cells, was first initiated at Site 1 and then successively at Sites 2-10 during a period of 2.7 s, as the capillary ripples propagated. These ripples appeared as concentric circular or oval rings (e.g. dashed rings in the figure), with a constant wavelength of about $\lambda_{cp} \sim$50 μm, characteristic for capillary waves (wavelength < 0.1 mm) observed on polymer films[19] and soft gels.[20] The characteristic attenuation time and length (the time and distance intervals respectively between the ripple initiation and diminishment) can be estimated from Videos 1 and 2 as $\tau \sim 1$ s and $\mu \sim 200$ μm, with $\mu \sim (\rho\gamma\lambda_{cp}^3)^{1/2}/\eta_s$ [21] where ρ is the density, γ the interfacial tension at the drop-air interface, and η_s the viscosity of the fluid layer mediating the ripples. de Gennes et al. [21] estimated that $\mu \approx 1$ cm for $\lambda_{cp} \approx 100$ μm on water. We assume that the drop surface layer contained the solvent (mostly chloroform) and the clusters which were a mixture of isobutyalamine but also trace amounts of water, methanol, and -Zn(OH). The exact composition and structure of the clusters and the surface layer are not known, and here

we take γ = 22.25 (isobutylamine) – 26.67 (chloroform) mN m^{-1} and ρ ~ 0.735 (isobutylamine) –1.49 (chloroform) g cm^{-3} as lower and upper limits of these quantities. We thus estimate η_s ~ 8.4 – 13 mPa s, which is ~20 times that of the viscosities of the solvents (~0.55 mPa s for chloroform) used. This is consistent with our proposed mechanism in which the drop surface was enriched with iZMC clusters due to the Marangoni flow and evaporation.

The diameters of BM cells at Sites 1-10 as a function time are plotted in **Figure 4i**, showing that the growth rate was fairly constant (~92±15 μm s^{-1}) for all the BM cells, much faster than the capillary flow rate (~0.1 μm s^{-1}) for creating coffee rings.[22] The development of a single BM cell at Site 1 was tracked in a series of magnified images (red circles in **Figure 4j-m**). The site appeared as a small spot at the beginning (indicated by the arrows in Figure 4h), around which the branched growth of filaments proceeded as a result of coalescence of the

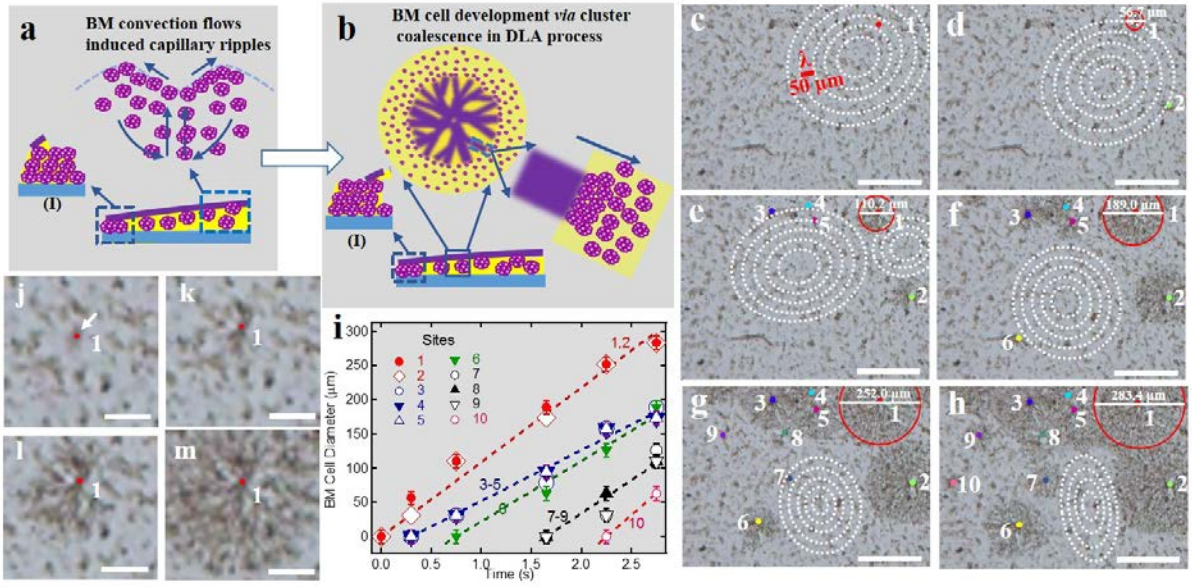

Figure 4 . Schematic images of capillary ripples and following BM cell development via cluster coalescence (a, b), and a series of images (c-h) extracted from Video 2 at time sequence of 0, 0.3, 0.75, 1.65, 2.25, and 2.7 s respectively. a, BM convection flows induced capillary ripples (schematically); b, BM cell formation via cluster coalescence in DLA process; i, the diameter of BM cells at ten site as a function of time, with the growth of the BM cell at Site 1 highlighted with red circles from b to f as an example; j-m, the magnified images of the site 1 in c, d, e and f, respectively. For the video microscopy experiment, 100 μL droplet containing 1 mg/mL ZnO nanoparticles (Supporting Figure 1) was dropped on the glass coverslip (1 mm×1 mm). The scale bars in are 200 μm in (c-h), and 50 μm in (j-m), respectively.

secondary clusters along radial BM flows (Figure 4b). The coalescence was likely mediated by inter-cluster solvophobic interactions. The dendritic growth of the cluster coalescence is characteristic of diffusion limited aggregation (DLA), [23] with the clusters arrested along radial BM flows forming gel-like residual patterns (Figure 4m and **Figure S5f**) comprising 3D swollen fibrillar network in dendritic morphologies. The ultimate BM cell size range (λ_{BM} =200-500 μm; *cf.* Figure 1d) is related to the Marangoni number $B = 32(\pi d/\lambda_{BM})^2$,[24] where the drop thickness d is of order 500 μm estimated from the drop volume and footprint. This gives B ~ 300–2000 (above the critical Marangoni number B_c = 80 for BM instabilities), with a corresponding Bénard velocity $U_{BM} \sim 0.4 – 2.6$ m s^{-1} which is consistent with the experimental value in a recent study [19]. To the first approximation $B \sim \eta^{-1}$ (η being the solvent viscosity), thus the different λ_{BM} values could be attributed to the inhomogeneity in the local viscosity and cluster concentration. Similarly, cluster coalescence also occurred upon rapid retreat of the contact line, causing dendritic growth of swollen filaments as the coffee ring formed (**Video 3** and Figure 4a (I), b(I)).

Upon further evaporation, the microscopic dendritic morphologies of gel-like residual patterns were retained, and the constituent filaments became more clearly defined. Lubrication by solvent molecules can facilitate spatial adjustment of iZMCs in the clusters, promoting formation of multilayered crystallites with square packing (Figure 2c). This evaporation driven, self-assembly based nucleation in transient aggregates significantly reduces the nucleation energy barrier, and crystallite formation occurs in a near spinodal regime,[25] with many crystallites forming simultaneously, leading to the polycrystalline structure in the solvated filaments. The final solvent removal drove rearrangement of the iZMCs to a lower energy configuration represented by multilayered crystallites with hexagonal packing (Figure 2d, e, f) in the ultimate polycrystalline filaments.

The dendrite morphological details in the residual pattern depended on the solvent composition and evaporation rate. For the solvent composition with V_{CM}:V_{iB} = 50:1 (**Figure 5 a-c**) or pure isobutylamine (**Figure 5d-f**) instead of V_{CM}:V_{iB} = 5:1 (cf. Figure 1), the overall surface patterns also comprised a central region surrounded by a coffee ring (Figure 5 a, d). However, the central cellular patterns resembled foliage of *Yucca gloriosa* (commonly known

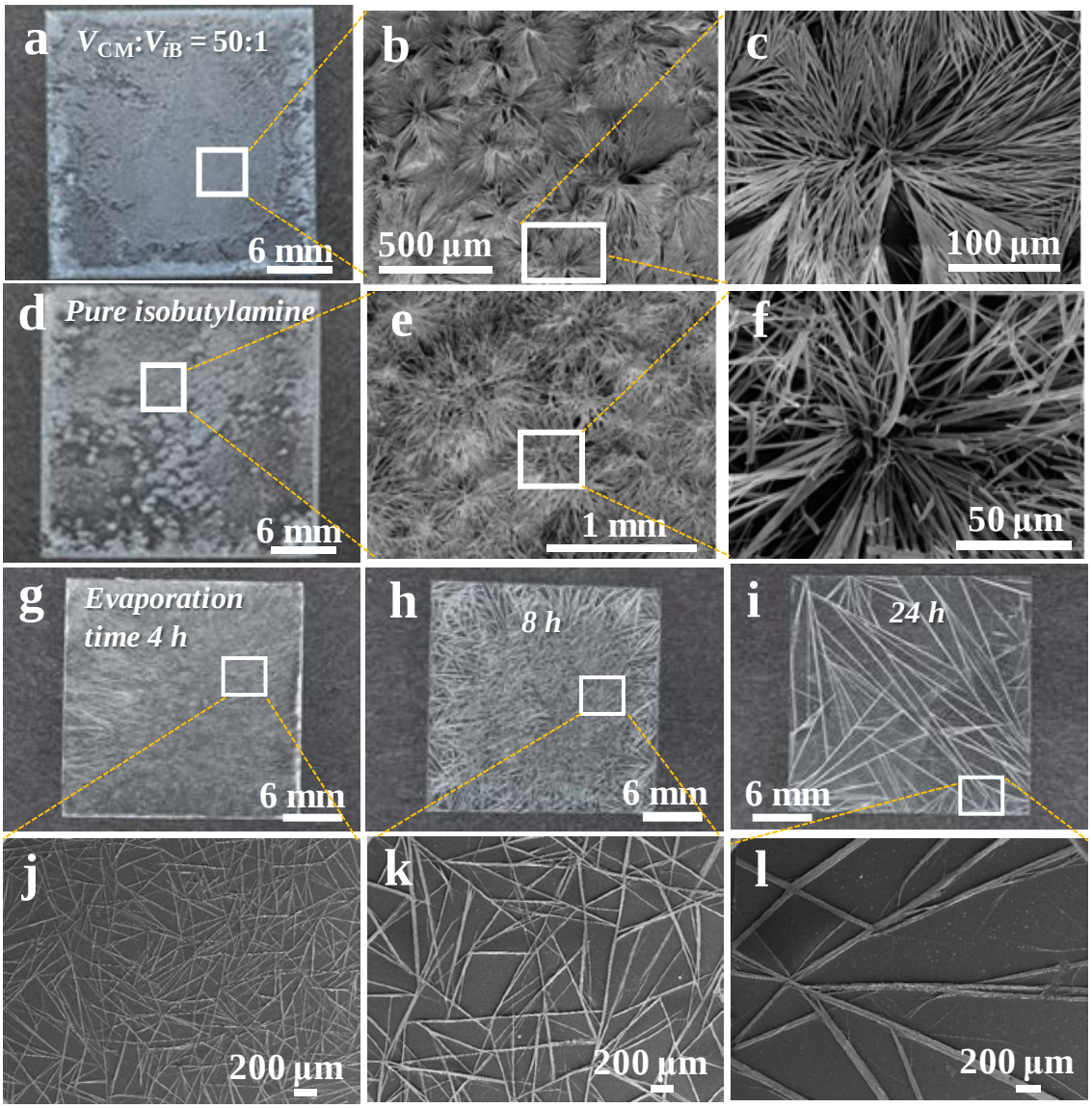

Figure 5. Photos and SEM images of residual patterns under different solvent compositions and slow evaporation. (**a-c**) The solvent compositions are V_{CM}:V_{iB} = 50:1; and (**d-f**) pure isobutylamine; with drying time ~ 20 min for both. For slow evaporation of a droplet (particle concentration 1 mg/mL; V_{CM}:V_{iB} = 5:1; 20 °C; RH ~ 65%), with evaporation time of (**g**) 4 h, (**h**) 8 h, (**i**) 24 h, the residual patterns appeared as interconnected fibre networks, with enlarged views in (**j**, **k**, **l**) corresponding to the white frames in (**g**, **h**, **i**), respectively. Note that the coffee ring just began to merge at evaporation time of 4 h (**g**), but was absent for slower evaporation (**h, l**).

as *Mound lily* or *Spanish dagger*) (Figure 5 b, c), with dendrites radiating from the centre and branches fanning radially outwards; or foliage of *Chlorophytum comosum* (commonly known as *spider plant*), with some broken or bent filaments and without ramification or branching (Figure 5e, f). For slow evaporation (*i.e.* with evaporation time of 4h, 8h and 24h, respectively; **Figure 5 g-l**), where the solvent flows were less pronounced, the residual patterns appeared as interconnected Microfilaments, with the coffee ring emerging at the 4 h evaporation time but absent for slower evaporation. Furthermore, the residual pattern also depended on the ZnO nanoparticle concentration and thus that of the *in situ* generated iZMC clusters (**Figure S8**). There existed a critical ZnO nanoparticle concentration (0.1 mg/mL) for the residual pattern with a central region of cellular patterns surrounded by a peripheral coffee ring; below which the residual pattern of random branched microfilaments was observed (Figure S8 a, b).

In conclusion, we report polycrystalline residual patterns upon fast evaporation of a mixed-solvent sessile drop containing ZnO nanoparticles, and explain our observations with a mechanism that accounts for the pattern structural hierarchy on nano-/micro-/macroscopic scales. The novelty of our observations (i.e. central cellular patterns surrounded by a peripheral coffee ring), and the challenge that we must meet in explaining them, is underpinned by the fact ZnO particles – unlike in previous droplet drying studies – are not inert but reactive. The molecular and particulate species generated in situ upon evaporative drying collude with and modify the solvent flows, as they undergo self-assembly and self-organisation under conditions far from equilibrium. As we report in a different report,[26] the complex residual pattern from a reactive ZnO nanofluids also depends on the nanoparticle morphology and crystallinity. Our results demonstrate the important role of the interplay between the *in situ* generated clusters from reactive ZnO nanoparticles and solvent flows in forming the hierarchical polycrystalline residual patterns. The proposed mechanism has implications to evaporation controlled self-organisation processes and surface pattern formation from a sessile drop containing reactive

nanoparticles, illustrating how different parameters (such as solvent composition, evaporation rate, particle concentration, and size) can be exploited to tailored the residual pattern.

Supplemental Material

Supporting Information is available online.

Acknowledgements

H.W. is supported by a Marie Skłodowska-Curie Individual Fellowship (Project Number 656830). W.H.B. would like to acknowledge funding from the EPSRC (EP/H034862/1, EP/G036780/1, EP/L016648/1, EP/K502996/1, EP/J500379/1) and Marie Curie Initial Training Network (MCITN) (NanoS3; Grant No. 290251). The authors thank J. Mantell (University of Bristol) for help with cryo-TEM. W.H.B would like to thank his plant loving Viking wife for helping to identify the plants resembling the micro-dendrites observed. All underlying data are provided within this paper and as supporting information accompanying this paper.

References

[1] aY. Luo, G. A. Braggin, G. T. Olson, A. R. Stevenson, W. L. Ruan, S. Zhang, *Langmuir* **2014**, *30*, 14631-14637; bX. Zhang, A. Crivoi, F. Duan, *Sci Rep* **2015**, *5*, 10926; cJ. Chen, S. Qin, X. Wu, A. P. Chu, *ACS Nano* **2016**, *10*, 832-838; dD. J. Harris, J. A. Lewis, *Langmuir* **2008**, *24*; eH. T. Wang, Z. B. Wang, L. M. Huang, A. Mitra, Y. S. Yan, *Langmuir* **2001**, *17*, 2572.

[2] R. D. Deegan, T. F. Dupont, G. Huber, S. R. Nager, T. A. Witten, *Nature* **1997**, *389*.

[3] L. E. Scrien, C. V. Sternling, *Nature* **1960**, *187*.

[4] aH. Hu, R. G. Larson, *Langmuir* **2005**, *21*, 3972; bM. Majumder, C. S. Rendall, J. A. Eukel, J. Y. Wang, N. Behabtu, C. L. Pint, T. Y. Liu, A. W. Orbaek, F. Mirri, J. Nam, A. R. Barron, R. H. Hauge, H. K. Schmidt, M. Pasquali, *J Phys Chem B* **2012**, *116*, 6536-6542; cX. Zhong, A. Crivoi, F. Duan, *Adv Colloid Interface Sci* **2015**, *217*, 13-30.

[5] aS. J. Vanhook, M. F. Duan, W. D. McCormick, J. B. Swift, H. L. Swiney, *Phys. Rev. Lett.* **1995**, *75*; bR. T. Gambaryan, *Adv. Colloid Interface Sci.* **2015**, *222*, 319; cV. X. Nguyen, K. J. Stebe, *Phys Rev Lett* **2002**, *88*, 164501.

[6] W. Han, Z. Lin, *Angewandte Chemie* **2012**, *51*, 1534-1546.

[7] A. Sukhanova, A. V. Baranov, T. S. Perova, J. H. Cohen, I. Nabiev, *Angew Chem Int Ed Engl* **2006**, *45*, 2048-2052.

[8] aP. J. Yunker, T. Still, M. A. Lohr, A. G. Yodh, *Nature* **2011**, *476*, 308-311; bT. Still, P. J. Yunker, A. G. Yodh, *Langmuir* **2012**, *28*, 4984-4988; cW. Sempels, R. De Dier, H. Mizuno, J. Hofkens, J. Vermant, *Nat Commun* **2013**, *4*, 1757.

[9] aZ. Liu, G. Zhang, Z. Cai, X. Chen, H. Luo, Y. Li, J. Wang, D. Zhang, *Adv Mater* **2014**, *26*, 6965-6977; bL. Zhang, H. Liu, Y. Zhao, X. Sun, Y. Wen, Y. Guo, X. Gao, C. A. Di, G. Yu, Y. Liu, *Adv Mater* **2012**, *24*, 436-440; cJ. Li, F. Ye, S. Vaziri, M. Muhammed, M. C. Lemme, M. Ostling, *Adv Mater* **2013**, *25*, 3985-3992.
[10] aZ. Liu, D. Qi, P. Guo, Y. Liu, B. Zhu, H. Yang, Y. Liu, B. Li, C. Zhang, J. Yu, B. Liedberg, X. Chen, *Adv Mater* **2015**, *27*, 6230-6237; bM. Layani, A. Kamyshny, S. Magdassi, *Nanoscale* **2014**, *6*, 5581-5591.
[11] N. Shahidzadeh, M. F. L. Schut, J. Desarnaud, M. Prat, D. Bonn, *Scientific reports* **2015**, *5*.
[12] aG. A. Pilkington, W. H. Briscoe, *Adv Colloid Interfac* **2012**, *179*, 68-84; bW. H. Briscoe, *Curr Opin Colloid In* **2015**, *20*, 46-53.
[13] aM. C. Biesinger, B. P. Payne, A. P. Grosvenor, L. W. M. Lau, A. R. Gerson, R. S. C. Smart, *Applied Surface Science* **2011**, *257*, 2717-2730; bT. Hirano, M. B. Andaloussi, U. Nagashima, P. Jensen, *J Chem Phys* **2014**, *141*, 094308.
[14] R. F. Thompson, M. Walker, C. A. Siebert, S. P. Muench, N. A. Ranson, *Methods* **2016**, *100*, 3-15.
[15] H. Wu, L. Chen, X. Zeng, T. Ren, W. H. Briscoe, *Soft Matter* **2014**, *10*, 5243-5248.
[16] T. Gilanyi, R. Meszaros, R. Varga, *Langmuir* **2000**, *16*.
[17] D. G. A. L. Aarts, M. Schmidt, H. N. W. Lekkerkerker, *Science* **2004**, *304*.
[18] aH. D. Ceniceros, *Physics of Fluids* **2003**, *15*, 245-256; bA. A. Golovin, A. A. Nepomnyashchy, L. M. Pismen, *Physics of Fluids* **1994**, *6*, 34-48; cX. Fanton, A. M. Cazabat, *Langmuir* **1998**, *14*.
[19] D. Bandyopadhyay, G. Singh, M. L. Becker, A. Karim, *ACS applied materials & interfaces* **2013**, *5*, 4006-4010.
[20] H. Kikuchi, K. Sakai, K. Takagi, *Physical Review B* **1994**, *49*, 3061-3065.
[21] P. G. de Gennes, W. F. Brochard, D. Quere, in *Capillarity and wetting phenomena: drope, bubbles, pearls, waves*, Springer, New York, **2004**, p. 240.
[22] R. D. Deegan, O. Bakajin, T. F. Dupont, G. Huber, S. R. N. T. A. Witten, *Phys. Rev. E.* **2000**, *62*.
[23] G. Daccord, R. Lenormand, *Nature* **1987**, *325*.
[24] J. R. A. Pearson, *Journal of Fluid Mechanics* **2006**, *4*.
[25] L. F. Filobelo, O. Galkin, P. G. Vekilov, *J Chem Phys* **2005**, *123*, 014904.
[26] P. Wasik, C. Redeker, T. G. Dane, A. M. Seddon, H. Wu, W. H. Briscoe, *Langmuir* **2018**, *34*, 1645-1654.
[27] See Supplemental Material at [URL will be inserted by publisher] for 1) ZnO nanoparticle preparation; 2) Confirmation of products from dissolution-reaction of ZnO nanoparticles during solvent evaporation; 3) Experimental protocol for Figure 2 and 3; 4) Sample preparation for TEM images in Figure 2d; and 5) Descriptions for Videos S1-S3.